ACS central science

http://pubs.acs.org/journal/acscii

Research Article

Bistable Photoswitch Allows in Vivo Control of Hematopoiesis

Lea Albert, Jatin Nagpal,[■] Wieland Steinchen,[■] Lei Zhang,[■] Laura Werel,[⬢] Nemanja Djokovic,[⬢] Dusan Ruzic, Malte Hoffarth, Jing Xu, Johanna Kaspareit, Frank Abendroth, Antoine Royant, Gert Bange, Katarina Nikolic, Soojin Ryu, Yali Dou, Lars-Oliver Essen, and Olalla Vázquez*

Cite This: *ACS Cent. Sci.* 2022, 8, 57−66

Read Online

ACCESS | Metrics & More | Article Recommendations | Supporting Information

ABSTRACT: Optical control has enabled functional modulation in cell culture with unparalleled spatiotemporal resolution. However, current tools for in vivo manipulation are scarce. Here, we design and implement a genuine *on*−*off* optochemical probe capable of achieving hematopoietic control in zebrafish. Our photopharmacological approach first developed conformationally strained visible light photoswitches (CS-VIPs) as inhibitors of the histone methyltransferase MLL1 (KMT2A). In blood homeostasis MLL1 plays a crucial yet controversial role. **CS-VIP 8** optimally fulfils the requirements of a true bistable functional system in vivo under visible-light irradiation, and with unprecedented stability. These properties are exemplified via hematopoiesis photoinhibition with a single isomer in zebrafish. The present interdisciplinary study uncovers the mechanism of action of CS-VIPs. Upon WDR5 binding, **CS-VIP 8** causes MLL1 release with concomitant allosteric rearrangements in the WDR5/RbBP5 interface. Since our tool provides on-demand reversible control without genetic intervention or continuous irradiation, it will foster hematopathology and epigenetic investigations. Furthermore, our workflow will enable exquisite photocontrol over other targets inhibited by macrocycles.

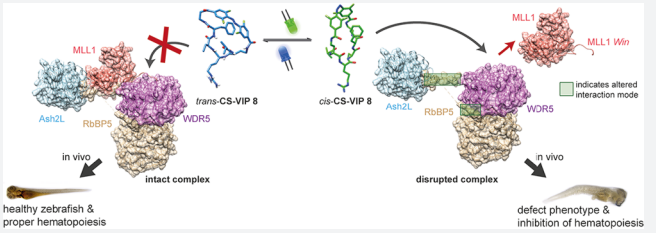

■ INTRODUCTION

The precise photocontrol of molecular activity to systematically trigger phenotypic traits opens unprecedented venues for in vivo elucidation of complex biological processes.[1,2] Since the first genetically encoded photoreceptors in neuroscience were developed,[3] the field has evolved. Now photopharmacology[4] controls functional outputs within unmodified targets bypassing gene delivery and has achieved in vivo modulation[5] of processes related to neurobiological phenomena like vision[6] and membrane transport[7,8] or, also, cytoskeleton dynamics.[9] However, these examples involve UV light and continuous irradiation and do not achieve the desirable *on*−*off* effect of photocages.[10]

Epigenetics coordinates gene expression responsible for balancing hematopoiesis. Its improper orchestration causes aberrant hematopoietic stem cell (HSC) differentiations and malfunction leading to hematological malignancies.[11] The histone methyltransferase MLL1 (KMT2A) entails the so-called MLL1 complex (MLL1, WDR5, RbBP5, Ash2L, DPY30), where subunit interactions control MLL1's activity. As chromatin-modifier, the MLL1 complex is vital for sustaining both hematopoiesis[12] and HSC self-renewal.[13] Furthermore, MLL1 is a potent oncogenic driver in hematopoietic cancers by influencing *HOX* gene expression. Interestingly, MLL1 may maintain its hematopoietic roles using mechanisms that do not depend on its histone methyltransferase (HMT) activity[14] but on protein−protein interactions (PPIs). The functional consequences of PPI modulations within the MLL1 complex remains elusive. To decode the complex biology underlying MLL1-dependent hematopoiesis, we require integrative approaches involving in vivo models, which are interrogated in highly controlled fashion. To our knowledge, there are no precedents of in vivo photocontrol of hematopoiesis. Such tools would elucidate the molecular mechanisms behind blood cell formation and may lead to novel therapeutics for hemopathies.

Herein, we report conformationally strained visible-light photoswitches (CS-VIPs), which allow quantitative functional conversion by visible-light irradiation in cell culture and zebrafish. CS-VIPs undergo exceptionally slow relaxation (five months) in aqueous solution. Employing crystallography, hydrogen−deuterium exchange mass spectrometry (HDX-MS), molecular dynamics (MD), and biological assays, we define their action mechanism on the MLL1 multiprotein complex. Importantly, our most potent photopharmacological agent, **CS-VIP 8**, is a true *on*−*off* switch that enables precise in vivo photocontrol over hematopoietic function without harsh UV light or wash-out.

Received: April 7, 2021
Published: December 22, 2021

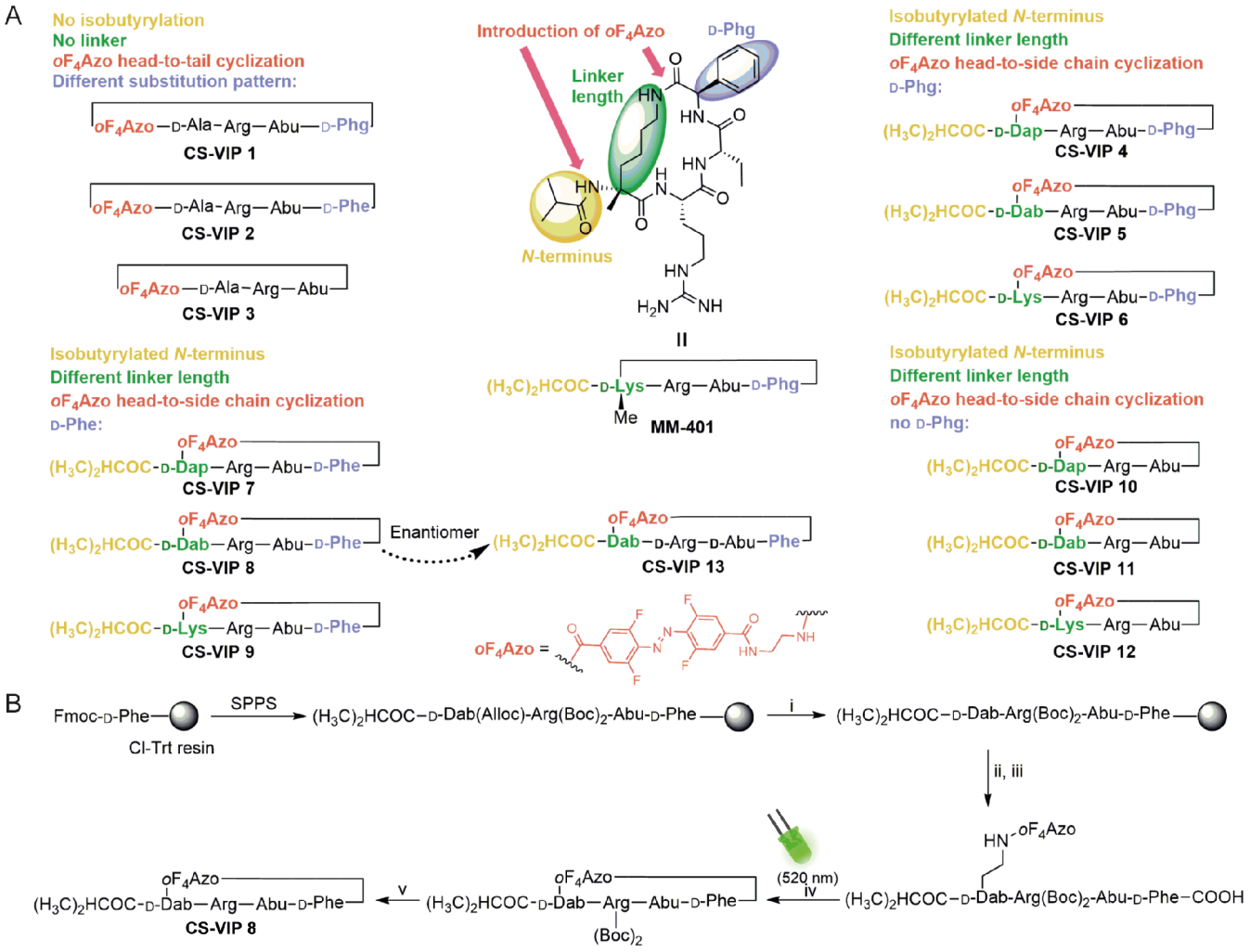

Figure 1. Design and synthesis of CS-VIPs. (A) Photoswitchable MM-401 cyclopeptides. (B) Exemplified synthesis for **CS-VIP 8**. (i) 1.00 equiv $Pd(PPh_3)_4$, 190 equiv morpholine, DCM, 2 h, rt; (ii) 4.00 equiv Oxyma, 4.00 equiv DIC, 4.00 equiv Mtt-oF_4Azo, DMF, 45 min, rt; (iii) HFIP/DCM 1:4, 2 h, rt; (iv) 3.00 equiv HATU, 4.00 equiv DIPEA, THF/DMF 98:2, 45 min, rt, at 520 nm 3 min; (v) 4 M HCl in dioxane, 3 h, rt; D-Dap D-diaminopropionic acid, D-Dab D-diaminobutyric acid, Abu aminobutyric acid, SPPS solid phase peptide synthesis.

RESULTS AND DISCUSSION

Design and Synthesis of the CS-VIPs. Recently, we reported in vitro MLL1 photocontrol, which ultimately affected leukemia cell proliferation.[15] However, the modest activity difference between isomers precluded in vivo experiments. We envisioned that the inclusion of a molecular transducer into a structurally defined scaffold should impart high conformational restraints and, thereby, achieve different biological output between photoisomers. The potent MLL1 inhibitor MM-401[16] (Figure 1A) is ideal to test if strained photoswitchable cyclopeptides can exert effective photomodulation of the molecular recognition process of MLL1 affecting in vivo hematopoiesis. As a photoswitch, we chose Hecht's oF_4Azo due to its excellent photochemical properties.[17] Initially, we explored 13 CS-VIPs (Figure 1A), which differed in oF_4Azo position, D-phenylglycine (D-Phg) presence, and ring size. D-Phg can epimerize; therefore, we considered its elimination and exchange by D-phenylalanine (D-Phe). Briefly, solid phase peptide synthesis (SPPS; Figure 1B) enabled our linear precursors where oF_4Azo was always on-resin incorporated at last, and arginine was Boc-protected to circumvent lability under Fmoc-deprotection[18] and Pbf side reactions,[19] respectively. Afterward, they were either head-to-tail or side-chain-to-tail cyclized at high dilution (1 mM) under irradiation at 520 nm for 3 min to steer the intramolecular product via *cis* isomerization.

Photochemical Characterization. As an illustrative example, the spectroscopic properties of **CS-VIP 8** were analyzed in detail (Figure 2). Its UV−vis spectra displayed the expected absorbance bands of oF_4Azo-containing compounds (Figure 2B).[18,20] Photoisomerization was fully reversible without photodegradation (Figure 2C). Interestingly, the thermodynamically unstable *cis* isomer is kinetically highly stable in organic solvents (oF_4Azo half-life: 700 days at rt in DMSO, 92 h at 60 °C in acetonitrile).[21] In contrast, thermal *cis* → *trans* conversion proceeds faster in water (oF_4Azo linear peptide *cis* content 86% at 520 nm photostationary state (PSS); 76% after 7 days).[18] Importantly, when oF_4Azo is incorporated into the conformationally restricted **CS-VIP 8**, its extraordinary stability was not only retained in water, but also surpassed nonrestricted oF_4Azo molecules[18,22] and unsubstituted azobenzene-containing cyclopeptides.[23] Indeed, our photoswitchable peptide maintained its equilibrium state by at least five months (Figure 2D,E). Notably, the 520 nm PSS achieved 95% *cis*-isomer (*cis*:*trans* 19:1), whereas the 405 nm

https://doi.org/10.1021/acscentsci.1c00434
ACS Cent. Sci. 2022, 8, 57−66

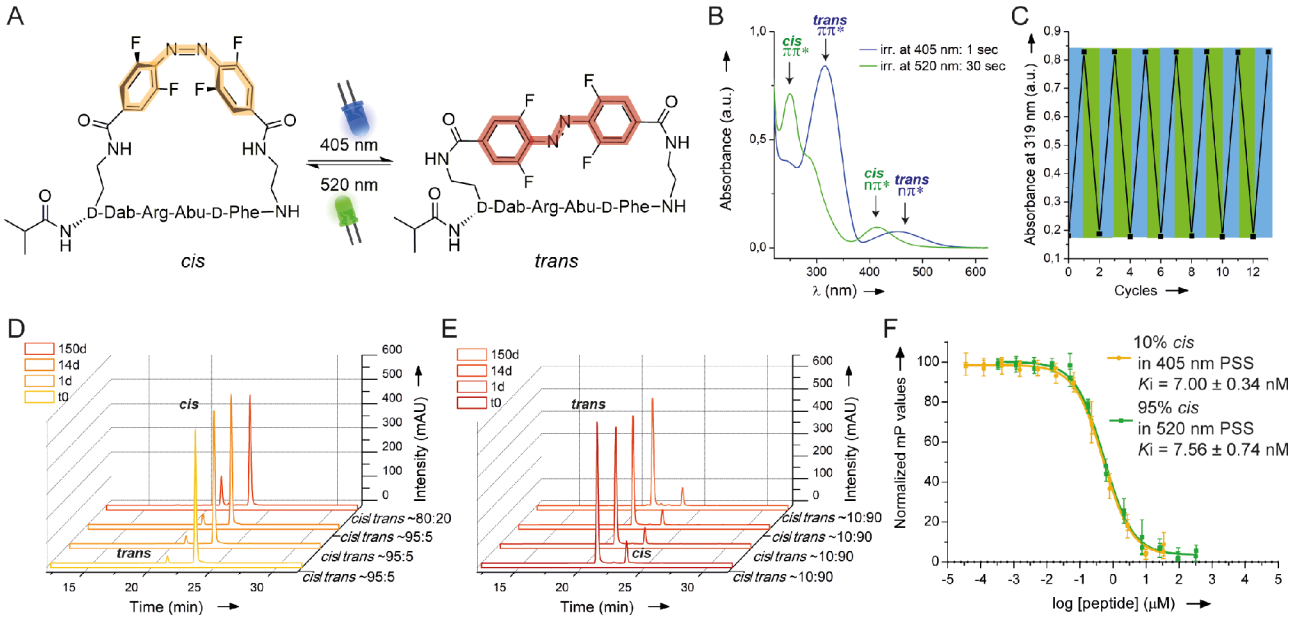

Figure 2. Photoisomerization studies of **CS-VIP 8** and interaction with WDR5. (A) Isomerization of **CS-VIP 8**. (B) UV−vis spectra in aqueous solution after irradiation at 405 and 520 nm reaching the PSS. (C) Reversible *cis*:*trans* cycles by alternating illumination at 405 (blue)/520 (green) nm. (D and E) Stability of the *cis*-isomer at the 520 nm PSS and the *trans* one at the 405 nm PSS, respectively, at rt in water via HPLC measurements. (F) Results of FP-based assays obtained by generating 405 and 520 nm PSS considering only the residual 10% of the *cis* isomer present in solution (yellow) and compared with the *cis*-state as obtained by illumination at 520 nm (green) including calculated K_i.

PSS formed a *cis*:*trans* mixture in a ratio of ∼1:10. Consequently, a switch between these PSS causes an ∼9.5/18-fold change of the *cis*/*trans*-isomer concentration, respectively. Finally, the stability against glutathione (GSH) was also improved (Figure S18). Preliminary photochemical studies of the other CS-VIPs showed similar behaviors.

Optimization of CS-VIP Binding to WDR5. Fluorescence polarization (FP) based assays revealed the binding of our CS-VIPs to WDR5 (Table 1, Figure S19). Importantly, *o*F_4Azo incorporation generally retained the parental nanomolar binding for most CS-VIPs (**4**−**9** and **11**). Affinity variations depended on substitution pattern, ring size, and the effective concentration of the binding-active isomer as set by the chosen PSS. **CS-VIPs 1**−**3**, without MM-401 isobutyrylated *N*-terminus displayed either no detectable (**CS-VIP 1** and **3**) or low micromolar (**CS-VIP 2**) binding. In silico experiments of **CS-VIPs 1** and **3** revealed that the key arginine is not inserted in WDR5 cavity (Figure S36). Our experiments reassert the positive effect of the isobutyrylated *N*-terminus on WDR5 binding affinity.

Considering CS-VIPs with the same ring size, the phenyl group is crucial for high affinities, i.e., **CS-VIP 10**−**12** devoid of this moiety displayed micromolar affinities and lacked light-dependent switching. In our virtual docking (VD), these binding poses were also ranked lower (Table S6, Figure S37) than the ones bearing D-Phg (**CS-VIP 4**−**6**, Figure S37) or D-Phe (**CS-VIP 7**−**9**, Figure S38). The D-Phe-containing CS-VIPs displayed the highest affinity differences between isomers. Also, for the inactive **CS-VIP 1**, the substitution of D-Phg for D-Phe (**CS-VIP 2**) increased affinity being consistent with VD (Table S6, Figure S36). In contrast to **CS-VIP 1** and **CS-VIP 3**, packing interactions between the arginine and the WDR5 residues F133, F263, and C261 could be predicted for **CS-VIP 2** (Figure S36). Consequently, our D-Phe modification not only improved CS-VIP synthetic accessibility but also functional properties.

Optimal ring size is decisive for maximizing both interaction and conformational changes between photoisomers. For us, calculated CHEMPLP values (Table S6) suggested that the 2-carbon linker (D-Dab) had the ideal length to supply the best **CS-VIPs**: **5** and **8**, which we verified experimentally (Table 1, Figure S19). The latter excels with an almost 10-fold switch of binding affinity. This agrees with the theoretical limit for a compound being only active in the *cis*-state. To confirm this, we adjusted the FP curve fit parameters to the effective *cis* concentration of **CS-VIP 8** (Figure 2F). We obtained an excellent concordance between the K_i values of the 520 nm PSS and the 405 nm PSS, when considering the residual *cis* isomer concentration (10%). Besides, when the samples were

Table 1. CS-VIP Inhibition Constants to WDR5 by FP-Based Competitive Assays[a]

CS-VIP	PSS at 405 nm K_i [μM]	PSS at 520 nm K_i [μM]	ratio
1	n.c.[c]	n.c.[c]	
2	∼3.35[b]	∼1.31[b]	2.56
3	n.c.[c]	n.c.[c]	
4	0.043 ± 0.006	0.079 ± 0.016	1.84
5	0.051 ± 0.010	0.008 ± 0.002	6.38
6	0.394 ± 0.023	0.239 ± 0.071	1.65
7	∼0.448[b]	0.104 ± 0.010	4.31
8	0.079 ± 0.004	0.008 ± 0.0008	9.88
9	0.831 ± 0.054	0.137 ± 0.012	6.07
10	∼1.10[b]	∼1.52[b]	1.38
11	0.688 ± 0.004	0.459 ± 0.060	1.50
12	∼3.69[b]	∼2.90[b]	1.27
13	∼19.3[b]	∼6.42[b]	3.00

[a]Mean values from at least two independent measurements (in triplicates); [fluorescent tracer] = 20 nM; fluorescent tracer K_d = 0.00104 ± 0.0005 μM.[15] [b]Estimated values due to a lack of the bottom plateau [c]Not calculable.

https://doi.org/10.1021/acscentsci.1c00434
ACS Cent. Sci. 2022, 8, 57−66

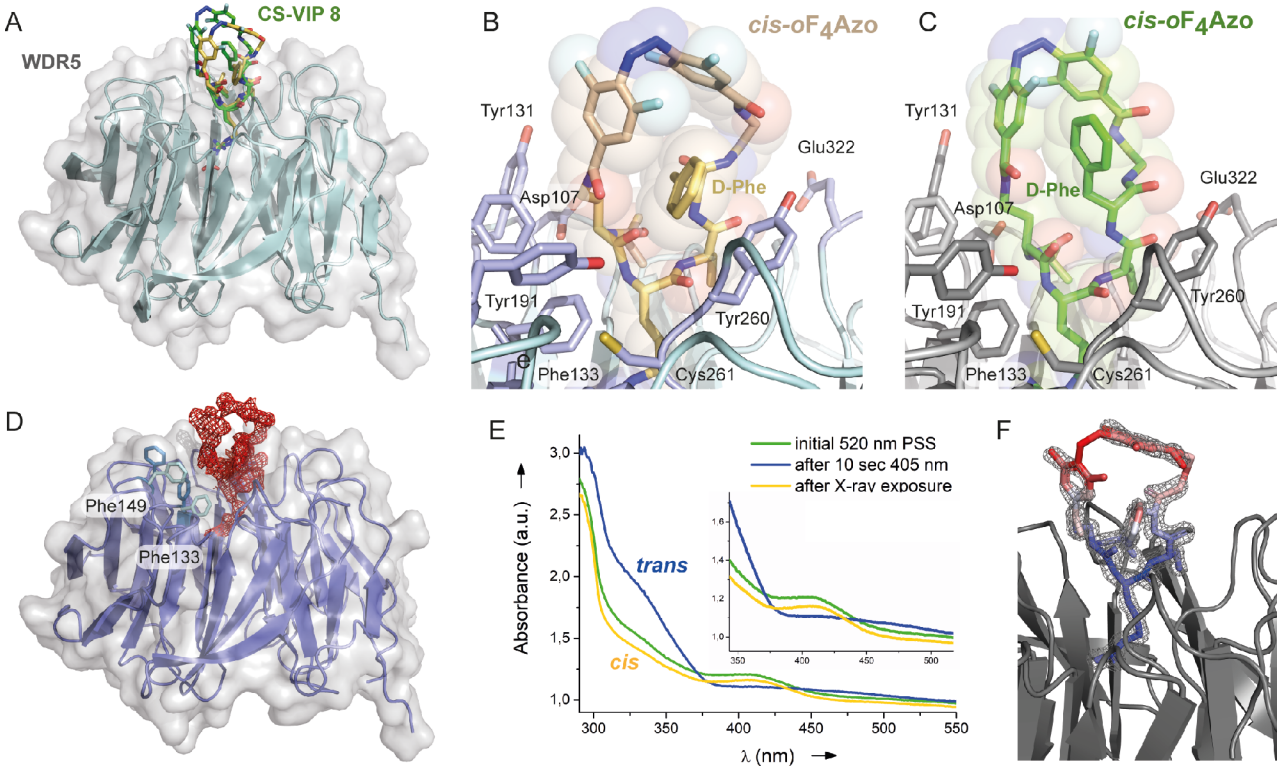

Figure 3. Structural characterization of WDR5•**CS-VIP 8** interaction. (A) Co-crystal structures of WDR5•**CS-VIP 8** complexes: overlay of *cis1* (**CS-VIP 8**: yellow) and *cis2* (**CS-VIP 8**: green) crystals. (B and C) WDR5-binding site for **CS-VIP 8** in crystal 1 (*cis1*) and in crystal 2 (*cis2*), respectively. (D) WDR5 apo-structure as generated by 405 nm illumination after crystallization. The shown $F_{obs,1} - F_{obs,2}$ difference electron density (red, contouring level 2σ) was calculated for *cis1*-apo states using phases of the *cis1* complex. Notably, Phe133 and Phe149 (marine blue apo; light cyan *cis1*) adopt a different conformation upon **CS-VIP 8** release. (E) Absorbance spectra of frozen WDR5 cocrystals recorded at the icOS Lab. (F) Binding site of the cryo-trapped structure from E; **CS-VIP 8** is colored as the B-factors range from 13 (blue) to 32 A^2 (red); the SIGMAA-weighted $2mF_{obs} - DF_{calc}$ electron density (gray) is shown at a contouring level of 2σ.

illuminated after WDR5 complexation (Figure S20), only the *trans* PSS mixture of **CS-VIP 8** isomerized to the *cis* isomer yielding comparable K_i values (Figure S20). In contrast, *cis* → *trans* photoisomerization is apparently slightly less effective when **CS-VIP 8** is bound to WDR5 (K_i 405 nm PSS = 64.7 nM; K_i *cis* → *trans* = 47.1 nM; Figure S20).

Taken all together, our **CS-VIP 8** variant is the most promising candidate for in vivo experiments as it maintains the nanomolar parental WDR5 affinity with an ∼10-fold difference between its photostationary isomers. These features significantly improved our previous results with photoresponsive linear peptides.[15,18] As for the MM-401 enantiomer,[16] the **CS-VIP 8** enantiomer, **CS-VIP 13**, exerted a 244/803-fold diminished binding to WDR5 relative to **CS-VIP 8** judging from its K_i values recorded at 405 and 520 nm PSSs, respectively.

Next, we determined the cocrystal structures of the WDR5•**CS-VIP 8** complex using different *cis*:*trans* ratios during crystallization (Figure 3). One by cocrystallization with **CS-VIP 8** set to a 1:10 *cis*:*trans* mixture formed by 405 nm PSS (*cis1*, PDB: 7AXS), the other with the predominant *cis* isomer formed at 520 nm PSS (*cis2*, PDB: 7AXP). Both states share an interaction mode that closely mimics MM-401 (PDB: 4GM9, Figure S27) along the isobutyryl-D-Dab-Arg-Abu-D-Phe motif. Interestingly, the superposition of these *cis*-**CS-VIP 8** complexes (Figure 3A) revealed different orientations of oF$_4$Azo and D-Phe. In the *cis1* crystal the D-Phe ring enables π-stacking contacts with Y260 like D-Phg in MM-401 while the *cis2* crystal has a higher solvent content and features less H-bonds and no π-stacking of *cis*-**CS-VIP 8** to Y260 (Figures 3B, S25). UV−vis microspectroscopy displayed only the *cis* isomer of **CS-VIP 8** within *cis1* crystals (Figure S28). To reveal structural consequences of *cis*:*trans* isomerization within complexes, we irradiated the *cis1* crystallization setups of WDR5•*cis*-**CS-VIP 8** after crystal formation at 405 nm to enforce *cis*:*trans* switching (PDB: 7AXU). UV−vis measurements verified *cis* → *trans* photoisomerization within the crystals (Figure S28). However, this procedure caused complete diffusion of **CS-VIP 8** out of WDR5-binding site as verified by a lack of electron density defining the ligand. (Figure 3D). Finally, we tested whether in crystallo irradiation at 405 nm of isolated cocrystals enables the intermediary states for the *off*-diffusion of the *trans*-**CS-VIP 8** isomer. In crystallo switching to *trans*-**CS-VIP 8** was observed by microspectroscopy at both 180 (Figure 3E) and 293 K (Figure S28). However, both structures (PDB: 7AXQ, 7AXX) apparently indicated X-ray mediated *trans* → *cis* back isomerization by displaying again the *cis*-**CS-VIP 8** within the binding site. This phenomenon was confirmed by microspectroscopic analysis after X-ray exposure (Figures 3F, S26, and S28). Similar X-ray induced structural changes within photoisomerisable chromophores have been observed before in the past, e.g. in the phytochromes Cph2[24] and PixJ.[25] We only observed increased thermal B factors for the oF$_4$Azo group, especially in the cocrystal cryo-trapped at 180 K. These observations corroborated our previous FP experiments, which were additionally substantiated by computational calculations (see SN1 in the SI). Overall, our biophysical analyses showed that only the *cis*-

https://doi.org/10.1021/acscentsci.1c00434
ACS Cent. Sci. 2022, 8, 57−66

CS-VIP 8 is active toward WDR5 and that the WDR5 presence increases the *trans* → *cis* isomerization due to its preference for the bound *cis* isomer (Figure S28D).

MLL1 Inhibition and Leukemogenesis Suppression. Compounds capable of effectively binding to WDR5 have displayed MLL1 inhibition by blocking MLL1/WDR5 interaction, which decrease leukemia cell proliferation.[26] In vitro functional radiometric HMT-assays with MLL1 complex (MLL1, WDR5, RbBP5, Ash2L) demonstrated that *cis*-**CS-VIP 8** is a potent inhibitor of MLL1 methylation activity with a 12-fold difference depending on illumination (IC_{50} 405 nm PSS = 9.20 ± 3.04 μM; IC_{50} 520 nm PSS = 0.792 ± 0.259 μM; Figure S21). Along these lines, we tested **CS-VIP 8**'s effect on leukemia-related cells (MOLM-13) after 2-day incubation at different PSSs. The poor cellular uptake of **CS-VIP 8** demanded pep-1 carrier as transfection method[27] and relatively high concentrations. Isomers are distinct compounds with different pharmacokinetic properties. To exclude that isomer differences could emerge due to artifacts from transfection, we included a washing step, which will confirm that observed cytotoxicity is only attributed to intracellular processes. Compared to the 405 nm PSS, our photoswitchable **CS-VIP 8** clearly gained inhibitory potency upon 520 nm irradiation in a dose-dependent manner (Figure 4A), which enabled the determination of its half-maximal inhibitory concentration (IC_{50}); i.e., 58.6 ± 1.6 μM (Figure 4B). However, under the same conditions, it was not possible to accurately obtain IC_{50} values for the *trans*-**CS-VIP 8** (Figure 4B), but this must be higher than 150 μM at least. These data clearly demonstrate that **CS-VIP 8** exhibits different isomer-dependent activities in MOLM-13 cells. In addition, we synthesized the enantiomer of **CS-VIP 8** where the key L-Arg was replaced by D-Lys (**CS-VIP 14**). This lacked any detectable WDR5 binding (Figure S19N); therefore, **CS-VIP 14** is a suitable control to evaluate the effect of the oF_4Azo itself without expecting any MLL1-dependent inhibition mechanism. Gratifyingly, the effect of *cis*-**CS-VIP 8** in MOLM-13 cells was the most potent one, and as occurred for *trans*-**CS-VIP 8**, the dose−response experiments of both **CS-VIP 14** isomers (Figure S22) could not be translated into accurate IC_{50} values under the same conditions (Figure 4B). These data suggest that the mechanism of the *cis*-**CS-VIP 8** is distinguishable from that of the WDR5-indepent **CS-VIP 14** analogs as well as *trans*-**CS-VIP 8**.

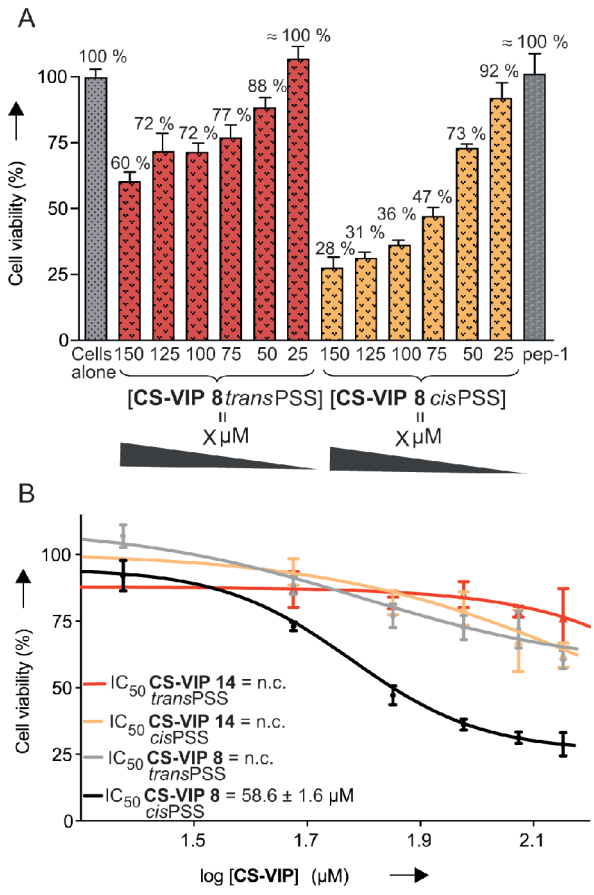

Figure 4. Dose−response toxicity of CS-VIPs on leukemia MOLM-13 cells. (A) Cell viability with both **CS-VIP 8** isomeric states for 2-day incubation; X: corresponding concentration. (B) IC_{50} determination of **CS-VIP 8** and **CS-VIP 14** in different isomeric states. All mean data points and standard deviations are derived from two independent experiments, and each concentration is in triplicate; n.c. not calculable.

***cis*-CS-VIP 8 Affects MLL1-Complex Assembly.** Despite the crucial contribution of MLL1 activity in regulating leukemia transcription programs, its HMT function could be dispensable for normal hematopoiesis.[14] However, depleting MLL1 components such as DPY30 and Ash2L displayed severe defects of lineage specification and differentiation.[28,29] Having established the structural basis of *cis*-**CS-VIP 8** binding to WDR5, we employed HDX-MS to corroborate our findings in solution by analyzing WDR5 in either the absence or presence of *cis*-**CS-VIP 8**. Hereby, regions of reduced H/D-exchange of WDR5 clustered around the binding site as evidenced by our crystal structures and virtual docking (Figures 5A and S29). We next studied *cis*-**CS-VIP 8**'s impact on the assembly of the whole MLL1 complex. Initially, we corroborated the integrity of the recombinant MLL1 complex. Thus, regions of reduced H/D-exchange correlated well with reported interaction interfaces (Figures S30−S34).[30] We then evaluated the H/D-exchange rates of the MLL1 complex with *cis*-**CS-VIP 8** and compared it with untreated MLL1. We obtained altered profiles for all components except DPY30 and mapped those differences onto available crystal structures (Figure 5B). The MLL1 polypeptide, *Win*, displayed increased H/D-exchange rates as well as the core of the MLL1 SET domain, suggesting interaction loss with WDR5 and RbBP5/Ash2L (Figures 5B and S30). Correspondingly, amino acids 336−354 of RbBP5 bridging between MLL1 and Ash2L exhibited likewise elevated H/D-exchange indicating that MLL1 is displaced from the complex by *cis*-**CS-VIP 8** (Figures 5B and S32). Conformational changes observed for Ash2L are in the proximity of its RbBP5/MLL1 interface (Figure S33), which further strengthens the notion of MLL1 release. Pull-down assays clearly indicated MLL1 vacating the complex in the presence of *cis*-**CS-VIP 8** (Figure S35). Although *cis*-**CS-VIP 8**-dependent H/D-exchange could not be detected at the *Win* binding site of WDR5, we postulate that this is due to opposing H/D-exchange differences induced by *cis*-**CS-VIP 8** binding (Figure 5A) and *Win* peptide release, roughly canceling each other. Notably, *cis*-**CS-VIP 8** induced elevated HDX in WDR5 residues 220−230, which are remote from the ligand binding site (Figures 5B and S31) and coincide with RbBP5-binding interface (PDB: 3P4F).[31] Our MD simulations, where a comparison of changes in solvent accessible surface areas (SASA) was conducted, verified that this region is indeed prone to deuterium exchange, as increased differences

https://doi.org/10.1021/acscentsci.1c00434
ACS Cent. Sci. 2022, 8, 57−66

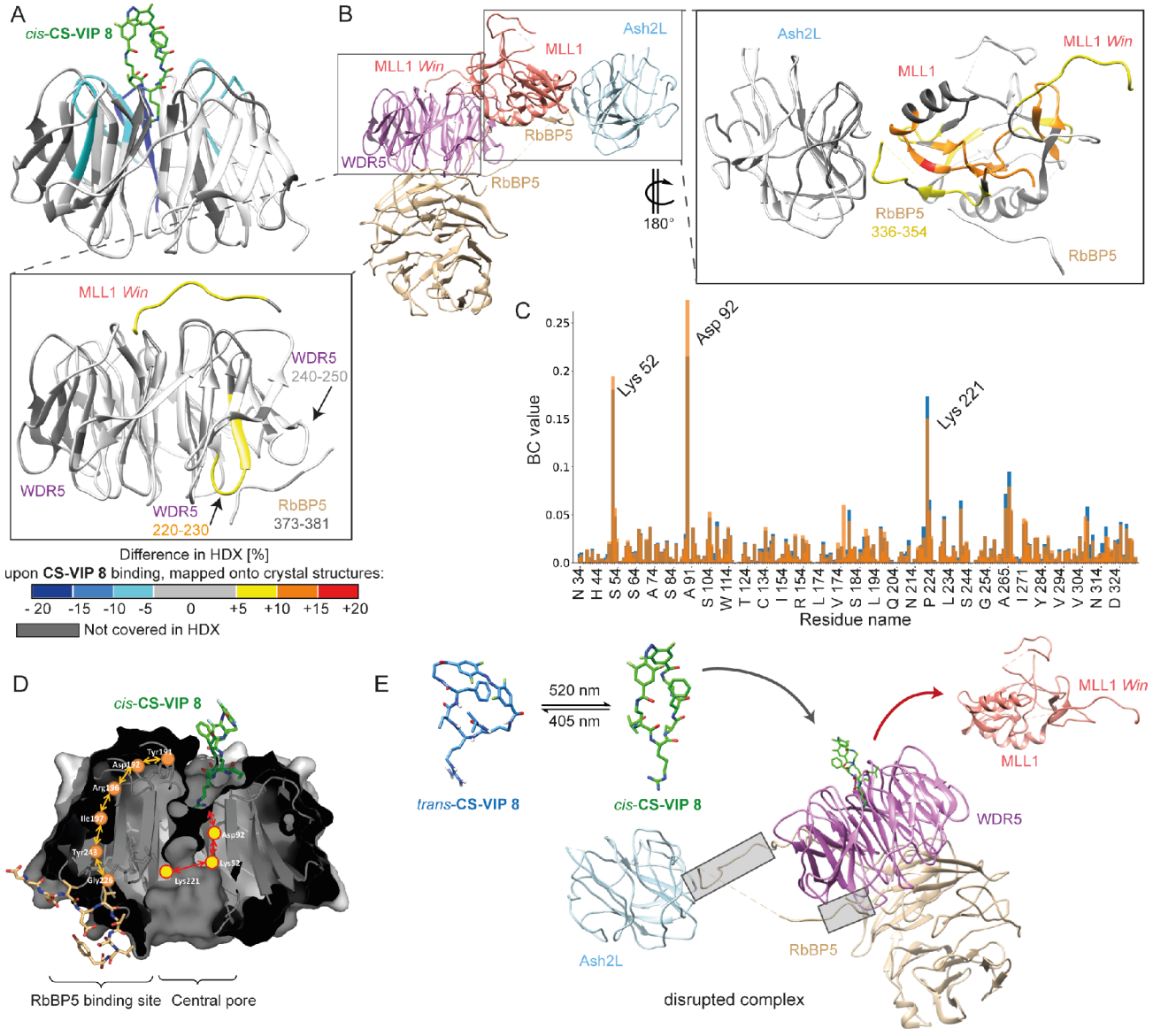

Figure 5. MLL1 complex disruption triggered by **CS-VIP 8** binding to WDR5 evaluated via HDX-MS and MD-studies. (A) Difference in D-uptake in WDR5 alone vs bound to *cis*-**CS-VIP 8** mapped onto our crystal structure (PDB: 7AXP). (B) 4-mer MLL1 complex structure (PDB: 6KIU);[32] WDR5 light purple, MLL1 salmon, RbBP5 tan, Ash2L light blue. (insets) Zoomed-in difference in D-uptake between with(out) **CS-VIP 8** addition mapped onto crystal structures of WDR5-MLL1-Win-RbBP5 (PDB: 3P4F)[31] and MLL1-RbBP5-Ash2L (PDB: 5F6L).[33] Dark gray regions represent amino acids that have not been covered in the HDX coverage map. (C) Betweenness-centrality (BC) values observed for MLL1-Win-WDR5-RbBP5 peptide (orange bars) and the *cis*-**CS-VIP 8**•WDR5-RbBP5 peptide (blue bars). (D) Schematic representation of **CS-VIP 8** mode of action displaying shortest paths connecting MLL1 and RbBP5 binding sites of residue interaction network identified through network analysis. (E) Model of **CS-VIP 8** mode of action. Gray boxes highlight altered interaction interfaces.

in SASA were calculated for hydrogens from peptide bonds of WDR5 alone vs WDR5•*cis*-**CS-VIP 8** (Figures S42 and SN2). Most importantly, conformational analysis of MD trajectories of the MLL1 complex either alone or complexed to *cis*-**CS-VIP 8** substantiated the partial unbinding of RbBP5 from WDR5 residues 220−230 during the course of MD simulation. We found that allosteric effects of *cis*-**CS-VIP 8** caused different dynamical behavior, for the MLL1 polypeptide, which resulted in partial unbinding of RbBP5 (Figures S41 and 43 and SN4). However, we conclude that complete dissociation of WDR5/RbBP5 is unlikely because no difference in deuterium uptake was observed at the second binding site of WDR5 to RbBP5 (residues 240−250, 289) upon *cis*-**CS-VIP 8** addition. As WDR5, RbBP5, and Ash2L still interacted in pull-down assays (Figure S35), this analysis suggests an altered structure of the remaining MLL1-devoid complex with *cis*-**CS-VIP 8.**

Allosteric Communication through WDR5. Further WDR5 analysis using perturbation-response scanning (PRS) revealed that "sensor regions", i.e., protein sites that are conformationally changed upon perturbation of effector residues, are positioned along the WDR5/RbBP5 interface, and effectors around its MLL1 binding site as in the central pore of WDR5 (Figure S43 and SN3). Thereby, we imply a direct allosteric communication between MLL1 and RbBP5 binding sites via WDR5, which indicates the importance of WDR5 as a mediator of RbBP5/MLL1 assembly in functional MLL1 complexes. Using graph-theory based residue interaction network analysis on conformational ensembles obtained

https://doi.org/10.1021/acscentsci.1c00434
ACS Cent. Sci. 2022, 8, 57−66

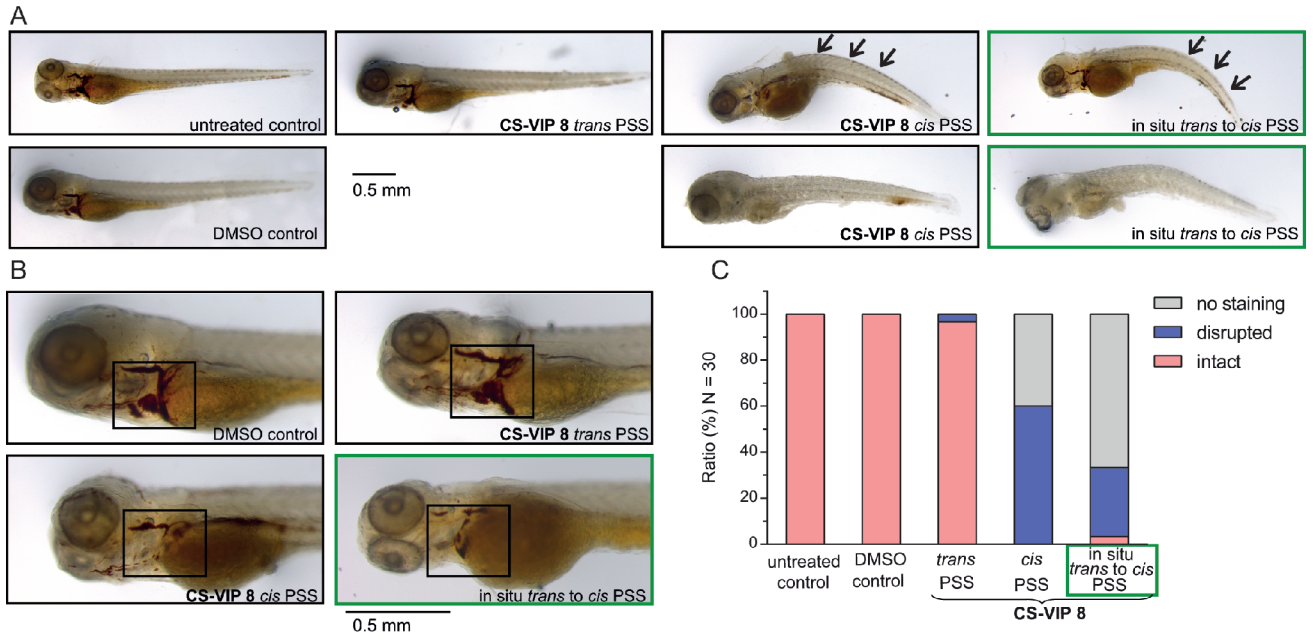

Figure 6. In vivo optochemical inhibition of hematopoiesis in 3-day postfertilization (dpf) zebrafish larvae. (A) Microscopy images of 3-dpf larvae incubated with 500 μM of **CS-VIP 8** at each PSS and controls. (B) Magnified micrographs of the heart region. (C) Bar chart comparing the blood flow of larvae incubated with **CS-VIP 8** and controls via analysis of *o*-dianisidine staining patterns, mean of three independent measurements. Arrows and rectangles highlight phenotypic changes.

by MD simulations, communication pathways between MLL1 and RbBP5 were studied. Betweenness centrality (BC) analysis of obtained networks (Figures 5C,D and S47 and SN4) revealed that WDR5 residues D92 and K52 at the MLL1 binding site, as well as RbBP5 binding residue K221, are contributors to the overall information flow along all derived networks (Figures 5C,D). This allosteric communication with the RbBP5 binding site through the central pore of WDR5 was recognized as the main cause of partial RbPB5 unbinding. Additionally, residues around Y191 were also identified to contribute for RbBP5 stabilization (Figure 5D, SN4, and Table S7), which coincides with increase of D-uptake of WDR5 residues 195−205 upon *cis*-**CS-VIP 8** binding, and the reported mutational analysis where Y191F was identified as a cause of low MLL1 activity.[34] All together, the activity loss with *cis*-**CS-VIP 8** apparently destabilizes the closed SET1 conformation, which uncovers the action mode of WDR5-binding inhibitors within the MLL1 complex (Figure 5E).

In Vivo Optochemical Control of Hematopoiesis. Encouraged by the on-target functional window for **CS-VIP 8** isomers and the severe disruption of MLL1 complex, we evaluated its potential for in vivo photomodulation of hematopoiesis. Genetic programs of hematopoiesis are highly conserved across vertebrates; therefore, we considered zebrafish as the best model because it is not only optically transparent but also encodes most of the functional domains of human *MLL1* gene products. Furthermore, Mll1 depletion in zebrafish causes severe defects related to hematopoiesis, such as lack of blood flow.[35] These phenotypes were detectable from day 2 onward by using morpholino (MO) mediated gene knockdown.[35] Indeed, it was between the third and fourth days postfertilization (dpf) when Wan et al.[35] observed the maximum reduced blood flow (78%) without lethality. This fact dictated our choice of larvae stage. Thus, once **CS-VIP 8** isomers reached their corresponding PSS in pure DMSO, each was diluted with egg water to a final concentration of 500 μM (1.5% DMSO). These solutions were directly added to 3-dpf larvae, which were previously treated with 1-phenyl-2-thiourea (PTU) to improve optical transparency and incubated for 18 h in darkness at 28.5 °C. Strikingly, only the *cis*-**CS-VIP 8** as obtained from the 520 nm PSS caused a complete lack of responsivity upon tail touch in the larvae, compared with untreated fish. Furthermore, under these experimental conditions, abnormal developmental phenotypes like curved body axis and heart edema were observed (Figure 6A,B). Remarkably, larvae incubated with either 1.5% DMSO or **CS-VIP 8** from 405 nm PSS (mainly the *trans* state) behaved as untreated ones, i.e., they were all alive with fast response to touch and without any apparent abnormalities. To quantify and determine whether these observed physiological changes were related to hematopoiesis, we performed three independent experiments, in which every condition was in duplicate containing five larvae per well (sample size, N = 30) and stained larvae with *o*-dianisidine for hemoglobin detection.[36] The staining pattern remained unaffected for the vehicle, i.e., 1.5% DMSO as well as for 97% of larvae incubated with **CS-VIP 8** at the 405 nm PSS. In contrast, staining with *cis*-**CS-VIP 8** was highly diminished (60%) or even absent (40%, Figure 6A,B). These reduced-blood flow and abnormal phenotypes coincide with antisense *mll1* knockdowns.[35] In addition, to provide greater confidence that the observed phenotypes are, indeed, due to Mll1 disruption, we conducted gene expression analysis using reverse transcription quantitative real-time PCR (RT-qPCR). It has been previously reported that MLL1 primarily regulates the expression of the genes *HOX7−11* (5′ in the *HOX* cluster), while expression of genes *HOX1−6* (3′ in the *HOX* cluster) is relatively unaffected by MLL1 activity.[37,38] Consequently, we evaluated the expression of both *hoxa9* and *hoxb5* genes (5′ and 3′ genes in the *hox* cluster, respectively) after the incubation of zebrafish embryos with **CS-VIP 8**. In line with our hypothesis, only the treatment with *cis*-**CS-VIP 8** led to a significant downregulation of expression of *hoxa9*

https://doi.org/10.1021/acscentsci.1c00434
ACS Cent. Sci. 2022, 8, 57−66

paralogs (*hoxa9a* and *hoxa9b*) while the expression of *hoxb5* remained unaltered (Figure S24). Notably, the embryos incubated with the *trans* isomer or the vehicle did not display these changes in the gene expression. Together with our structural data, which display specific MLL1 complex disruption, these functional data strongly support that only the *cis*-**CS-VIP 8** can affect hematopoiesis in vivo.

Finally, to release the full potential of our photoresponsive probes, we explored the possibility to externally control the in vivo inhibition of hematopoiesis via on-demand photoactivation. Thus, larvae incubated with the innocuous *trans*-**CS-VIP 8** for 1 h were irradiated in situ at 520 nm for 30 s. After 18 h incubation, we detected effects comparable to the positive control, where larvae were exposed to *cis*-**CS-VIP 8**. Precisely, only 3% of larvae displayed an intact *o*-dianisidine staining pattern while in the remainder labeling was either partially disrupted (30%) or completely affected (67%). Negative controls of untreated fish or vehicle (1.5% DMSO) verified the harmlessness of visible-light irradiation (Figure S23). Taken together, we first developed a light-controlled enzyme modulator capable of achieving in vivo optochemical control of hematopoiesis, to our knowledge.

Concluding Remarks. Our understanding of gene regulatory mechanisms at the molecular level is often limited due to the lack of in vivo structure−function studies that can cope with the redundancy and ubiquitous expression of chromatin-modifying complexes. In this context, our work provides a successful proof-of-concept of in vivo photopharmacology to gain insight into the hematopoietic function of the MLL1 complex. We introduced the family of conformationally strained visible-light photoswitches (CS-VIPs) that can not only tightly interact with WDR5 but also light-control in vivo hematopoiesis in zebrafish without additional genetic modification. Our exhaustive molecular studies provide a detailed view on the action of MLL1−WDR5 inhibitors in the context of the intact MLL1 complex. Upon **CS-VIP 8** binding to WDR5, MLL1 dissociates from the core-complex, while the remaining complex subunits undergo conformational changes, e.g., by rewiring residues interaction networks in the WDR5−RbBP5 binding interface. Given the advent of time-resolved crystallography techniques like serial synchrotron crystallography (SSC)[39] our WDR5•**CS-VIP 8** cocrystals represent now a highly promising model system for studying the *cis* → *trans* conversion of cyclic azopeptides in crystallo with their concomitant off/on diffusion from the protein target.

Our in vivo 3-dpf larvae zebrafish experiments displayed abnormal developmental traits such as hematopoiesis staining deficits, complete lack of responsivity, curved body axis, heart edema, and death preferentially upon *cis*-**CS-VIP 8** addition. These phenotypic changes together with our RT-qPCR, which demonstrated robust reduction of *hoxa9a/b* gene expression while *hoxb5a* gene one remained unaffected at the same development stage, link the in vivo effects of *cis*-**CS-VIP 8** with the specific inhibition of Mll1 activity. These observations suggest that the toxicity in the leukemia-related cells may be MLL1-dependent as well. However, to fully understand these complex biological mechanisms further in-depth investigations will be conducted where reporter genes assays as well as earlier stages of development will be studied. In our opinion this work marks a first step into the uncharted territory of hematopoiesis photopharmacology as well as in vivo light-controlled epigenetics. Furthermore, although the proof-of-concept application of our CS-VIPs was to unravel MLL1-related hematopoiesis, we expect our compounds to find further applications in diverse areas where in situ temporal control of MLL1 architecture is required or in which, β-propeller proteins, such as WDR5, act as interactions hubs.[40] Our methodology goes beyond the traditional reductionist mindset for dissecting biological systems, providing new tools for analyzing the assembly of complex biological machineries. This workflow can be readily expanded for other druggable targets and will increase the scarce toolbox of light-controlled enzyme modulators. Finally, both the implication of epigenetics in the development of hematopoietic malignancies and the appearance of epigenetic modifiers in clinical trials provides a perfect timeline for exploiting the modulation of hematopoiesis via epigenetic networks.

■ ASSOCIATED CONTENT

Supporting Information

The Supporting Information is available free of charge at https://pubs.acs.org/doi/10.1021/acscentsci.1c00434.

General procedures, characterization and supplementary figures, tables, and notes (PDF)

■ AUTHOR INFORMATION

Corresponding Author

Olalla Vázquez − *Department of Chemistry, University of Marburg, 35037 Marburg, Germany; Center for Synthetic Microbiology (SYNMIKRO), University of Marburg, 35037 Marburg, Germany;* orcid.org/0000-0002-7555-1865; Email: olalla.vazquez@staff.uni-marburg.de

Authors

Lea Albert − *Department of Chemistry, University of Marburg, 35037 Marburg, Germany*

Jatin Nagpal − *APC Microbiome Ireland, University College Cork, Cork, Ireland*

Wieland Steinchen − *Department of Chemistry, University of Marburg, 35037 Marburg, Germany; Center for Synthetic Microbiology (SYNMIKRO), University of Marburg, 35037 Marburg, Germany*

Lei Zhang − *Department of Chemistry, University of Marburg, 35037 Marburg, Germany*

Laura Werel − *Department of Chemistry, University of Marburg, 35037 Marburg, Germany*

Nemanja Djokovic − *Department of Pharmaceutical Chemistry, University of Belgrade, 11000 Belgrade, Serbia;* orcid.org/0000-0001-9972-3492

Dusan Ruzic − *Department of Pharmaceutical Chemistry, University of Belgrade, 11000 Belgrade, Serbia*

Malte Hoffarth − *Department of Chemistry, University of Marburg, 35037 Marburg, Germany*

Jing Xu − *Department of Pathology, University of Michigan, Ann Arbor, Michigan 48109, United States*

Johanna Kaspareit − *University Medical Center, Johannes Gutenberg University Mainz, 55122 Mainz, Germany*

Frank Abendroth − *Department of Chemistry, University of Marburg, 35037 Marburg, Germany*

Antoine Royant − *Univ. Grenoble Alpes, CNRS, CEA, Institut de Biologie Structurale (IBS), 38044 Grenoble, France; European Synchrotron Radiation Facility, 38043 Grenoble, France*

https://doi.org/10.1021/acscentsci.1c00434
ACS Cent. Sci. 2022, 8, 57−66

Gert Bange − *Department of Chemistry, University of Marburg, 35037 Marburg, Germany; Center for Synthetic Microbiology (SYNMIKRO), University of Marburg, 35037 Marburg, Germany*

Katarina Nikolic − *Department of Pharmaceutical Chemistry, University of Belgrade, 11000 Belgrade, Serbia*

Soojin Ryu − *University Medical Center, Johannes Gutenberg University Mainz, 55122 Mainz, Germany; Living Systems Institute, University of Exeter, Exeter EX4 QD, U.K.; College of Medicine and Health, University of Exeter, Exeter EX4 4PY, U.K.*

Yali Dou − *Norris Comprehensive Cancer Center, University of Southern California, Los Angeles, California 90007, United States;* orcid.org/0000-0002-4040-1429

Lars-Oliver Essen − *Department of Chemistry, University of Marburg, 35037 Marburg, Germany; Center for Synthetic Microbiology (SYNMIKRO), University of Marburg, 35037 Marburg, Germany;* orcid.org/0000-0003-4272-4026

Complete contact information is available at: https://pubs.acs.org/10.1021/acscentsci.1c00434

Author Contributions

■J.N., W.S., and L.Z. contributed equally to this work.

Author Contributions

●L.W. and N.D. contributed equally to this work.

Notes

The authors declare no competing financial interest.

■ ACKNOWLEDGMENTS

We dedicate this article to Prof. J. L. Mascareñas on the occasion of his 60th birthday. We thank Prof. Dr. E. Meggers for access to the cell laboratory; Dr. V. Srinivasan for initial crystallization attempts; P. Erramsetti and Dr. Y. Wang for assisting with the MOLM-13 cell line from Zentrum für Tumor und Immun-biologie (UMR) and Prof. A. E. Hargrove for critical feedback (Duke University). We acknowledge the DFG for cofinancing the AccuTOF GCv 4G (JEOL) Time of Flight (TOF) mass spectrometer (INST 160/622-1 FUGG) and the Institute of Molecular Biology (IMB, Mainz, Germany) Microscopy Core Facility. Numerical simulations were run on the PARADOX-IV supercomputing facility at the Scientific Computing Laboratory, National Center of Excellence for the Study of Complex Systems, Institute of Physics Belgrade, supported in part by the Ministry of Education, Science, and Technological Development of the Republic of Serbia under project no. ON171017. N.D., D.R., and K.N. acknowledge the project of the Ministry of Science and Technological Development of the Republic of Serbia for the Faculty of Pharmacy, University of Belgrade, no. 451-03-9/2021-14/200161. A.R. acknowledges the ic/OS platform of the Grenoble Instruct-ERIC center (ISBG; UMS 3518 CNRS-CEA-UGA-EMBL) within the Grenoble Partnership for Structural Biology (PSB), supported by FRISBI (ANR-10-INBS-05-02) and GRAL, financed within the University Grenoble Alpes graduate school (Ecoles Universitaires de Recherche) CBH-EUR-GS (ANR-17-EURE-0003). Finally, this work was financially supported by DFG programs: SPP1926 "Next Generation Optogenetics": Young Investigator program (grant no. GO1011/11-1), TRR81: "Chromatin Changes in Differentiation and Malignancies" (TRR81/3, Z04), and "Control of epigenetic states through light-triggered protein−protein interaction mediators" (grant no. VA 1002/5-1).

■ REFERENCES

(1) Ankenbruck, N.; Courtney, T.; Naro, Y.; Deiters, A. Optochemical Control of Biological Processes in Cells and Animals. *Angew. Chem., Int. Ed.* **2018**, *57* (11), 2768−2798.

(2) Gautier, A.; Gauron, C.; Volovitch, M.; Bensimon, D.; Jullien, L.; Vriz, S. How to control proteins with light in living systems. *Nat. Chem. Biol.* **2014**, *10* (7), 533−41.

(3) Deisseroth, K. Controlling the brain with light. *Sci. Am.* **2010**, *303* (5), 48−55.

(4) Borowiak, M.; Kullmer, F.; Gegenfurtner, F.; Peil, S.; Nasufovic, V.; Zahler, S.; Thorn-Seshold, O.; Trauner, D.; Arndt, H. D. Optical Manipulation of F-Actin with Photoswitchable Small Molecules. *J. Am. Chem. Soc.* **2020**, *142* (20), 9240−9249.

(5) Hull, K.; Morstein, J.; Trauner, D. In Vivo Photopharmacology. *Chem. Rev.* **2018**, *118* (21), 10710−10747.

(6) Polosukhina, A.; Litt, J.; Tochitsky, I.; Nemargut, J.; Sychev, Y.; De Kouchkovsky, I.; Huang, T.; Borges, K.; Trauner, D.; Van Gelder, R. N.; Kramer, R. H. Photochemical restoration of visual responses in blind mice. *Neuron* **2012**, *75* (2), 271−82.

(7) Pittolo, S.; Gomez-Santacana, X.; Eckelt, K.; Rovira, X.; Dalton, J.; Goudet, C.; Pin, J. P.; Llobet, A.; Giraldo, J.; Llebaria, A.; Gorostiza, P. An allosteric modulator to control endogenous G protein-coupled receptors with light. *Nat. Chem. Biol.* **2014**, *10* (10), 813−5.

(8) Lam, P. Y.; Thawani, A. R.; Balderas, E.; White, A. J. P.; Chaudhuri, D.; Fuchter, M. J.; Peterson, R. T. TRPswitch-A Step-Function Chemo-optogenetic Ligand for the Vertebrate TRPA1 Channel. *J. Am. Chem. Soc.* **2020**, *142* (41), 17457−17468.

(9) Borowiak, M.; Nahaboo, W.; Reynders, M.; Nekolla, K.; Jalinot, P.; Hasserodt, J.; Rehberg, M.; Delattre, M.; Zahler, S.; Vollmar, A.; Trauner, D.; Thorn-Seshold, O. Photoswitchable Inhibitors of Microtubule Dynamics Optically Control Mitosis and Cell Death. *Cell* **2015**, *162* (2), 403−411.

(10) Uhl, E.; Wolff, F.; Mangal, S.; Dube, H.; Zanin, E. Light-Controlled Cell-Cycle Arrest and Apoptosis. *Angew. Chem., Int. Ed.* **2021**, *60* (3), 1187−1196.

(11) Chung, Y. R.; Schatoff, E.; Abdel-Wahab, O. Epigenetic alterations in hematopoietic malignancies. *Int. J. Hematol.* **2012**, *96* (4), 413−27.

(12) Artinger, E. L.; Mishra, B. P.; Zaffuto, K. M.; Li, B. E.; Chung, E. K.; Moore, A. W.; Chen, Y.; Cheng, C.; Ernst, P. An MLL-dependent network sustains hematopoiesis. *Proc. Natl. Acad. Sci. U. S. A.* **2013**, *110* (29), 12000−5.

(13) McMahon, K. A.; Hiew, S. Y.; Hadjur, S.; Veiga-Fernandes, H.; Menzel, U.; Price, A. J.; Kioussis, D.; Williams, O.; Brady, H. J. Mll has a critical role in fetal and adult hematopoietic stem cell self-renewal. *Cell Stem Cell* **2007**, *1* (3), 338−45.

(14) Mishra, B. P.; Zaffuto, K. M.; Artinger, E. L.; Org, T.; Mikkola, H. K.; Cheng, C.; Djabali, M.; Ernst, P. The histone methyltransferase activity of MLL1 is dispensable for hematopoiesis and leukemogenesis. *Cell Rep.* **2014**, *7* (4), 1239−47.

(15) Albert, L.; Xu, J.; Wan, R.; Srinivasan, V.; Dou, Y.; Vazquez, O. Controlled inhibition of methyltransferases using photoswitchable peptidomimetics: towards an epigenetic regulation of leukemia. *Chem. Sci.* **2017**, *8* (6), 4612−4618.

(16) Cao, F.; Townsend, E. C.; Karatas, H.; Xu, J.; Li, L.; Lee, S.; Liu, L.; Chen, Y.; Ouillette, P.; Zhu, J.; Hess, J. L.; Atadja, P.; Lei, M.; Qin, Z. S.; Malek, S.; Wang, S.; Dou, Y. Targeting MLL1 H3K4 methyltransferase activity in mixed-lineage leukemia. *Mol. Cell* **2014**, *53* (2), 247−61.

(17) Bleger, D.; Schwarz, J.; Brouwer, A. M.; Hecht, S. o-Fluoroazobenzenes as readily synthesized photoswitches offering nearly quantitative two-way isomerization with visible light. *J. Am. Chem. Soc.* **2012**, *134* (51), 20597−600.

(18) Albert, L.; Penalver, A.; Djokovic, N.; Werel, L.; Hoffarth, M.; Ruzic, D.; Xu, J.; Essen, L. O.; Nikolic, K.; Dou, Y.; Vazquez, O.

Modulating Protein-Protein Interactions with Visible-Light-Responsive Peptide Backbone Photoswitches. *ChemBioChem* **2019**, *20* (11), 1417−1429.
(19) Schutt, M.; Krupka, S. S.; Milbradt, A. G.; Deindl, S.; Sinner, E. K.; Oesterhelt, D.; Renner, C.; Moroder, L. Photocontrol of cell adhesion processes: model studies with cyclic azobenzene-RGD peptides. *Chem. Biol.* **2003**, *10* (6), 487−90.
(20) Zhang, L.; Linden, G.; Vazquez, O. In search of visible-light photoresponsive peptide nucleic acids (PNAs) for reversible control of DNA hybridization. *Beilstein J. Org. Chem.* **2019**, *15*, 2500−2508.
(21) Knie, C.; Utecht, M.; Zhao, F.; Kulla, H.; Kovalenko, S.; Brouwer, A. M.; Saalfrank, P.; Hecht, S.; Bleger, D. ortho-Fluoroazobenzenes: visible light switches with very long-Lived Z. isomers. *Chem. - Eur. J.* **2014**, *20* (50), 16492−501.
(22) Aggarwal, K.; Kuka, T. P.; Banik, M.; Medellin, B. P.; Ngo, C. Q.; Xie, D.; Fernandes, Y.; Dangerfield, T. L.; Ye, E.; Bouley, B.; Johnson, K. A.; Zhang, Y. J.; Eberhart, J. K.; Que, E. L. Visible Light Mediated Bidirectional Control over Carbonic Anhydrase Activity in Cells and in Vivo Using Azobenzenesulfonamides. *J. Am. Chem. Soc.* **2020**, *142* (34), 14522−14531.
(23) Renner, C.; Kusebauch, U.; Loweneck, M.; Milbradt, A. G.; Moroder, L. Azobenzene as photoresponsive conformational switch in cyclic peptides. *J. Pept. Res.* **2005**, *65* (1), 4−14.
(24) Anders, K.; Daminelli-Widany, G.; Mroginski, M. A.; von Stetten, D.; Essen, L. O. Structure of the cyanobacterial phytochrome 2 photosensor implies a tryptophan switch for phytochrome signaling. *J. Biol. Chem.* **2013**, *288* (50), 35714−25.
(25) Burgie, E. S.; Clinger, J. A.; Miller, M. D.; Brewster, A. S.; Aller, P.; Butryn, A.; Fuller, F. D.; Gul, S.; Young, I. D.; Pham, C. C.; Kim, I. S.; Bhowmick, A.; O'Riordan, L. J.; Sutherlin, K. D.; Heinemann, J. V.; Batyuk, A.; Alonso-Mori, R.; Hunter, M. S.; Koglin, J. E.; Yano, J.; Yachandra, V. K.; Sauter, N. K.; Cohen, A. E.; Kern, J.; Orville, A. M.; Phillips, G. N., Jr.; Vierstra, R. D. Photoreversible interconversion of a phytochrome photosensory module in the crystalline state. *Proc. Natl. Acad. Sci. U. S. A.* **2020**, *117* (1), 300−307.
(26) Wang, Z. H.; Li, D. D.; Chen, W. L.; You, Q. D.; Guo, X. K. Targeting protein-protein interaction between MLL1 and reciprocal proteins for leukemia therapy. *Bioorg. Med. Chem.* **2018**, *26* (2), 356−365.
(27) Morris, M. C.; Depollier, J.; Mery, J.; Heitz, F.; Divita, G. A peptide carrier for the delivery of biologically active proteins into mammalian cells. *Nat. Biotechnol.* **2001**, *19* (12), 1173−6.
(28) Yang, Z.; Augustin, J.; Chang, C.; Hu, J.; Shah, K.; Chang, C. W.; Townes, T.; Jiang, H. The DPY30 subunit in SET1/MLL complexes regulates the proliferation and differentiation of hematopoietic progenitor cells. *Blood* **2014**, *124* (13), 2025−33.
(29) Luscher-Firzlaff, J.; Chatain, N.; Kuo, C. C.; Braunschweig, T.; Bochynska, A.; Ullius, A.; Denecke, B.; Costa, I. G.; Koschmieder, S.; Luscher, B. Hematopoietic stem and progenitor cell proliferation and differentiation requires the trithorax protein Ash2l. *Sci. Rep* **2019**, *9* (1), 8262.
(30) Kaustov, L.; Lemak, A.; Wu, H.; Faini, M.; Fan, L.; Fang, X.; Zeng, H.; Duan, S.; Allali-Hassani, A.; Li, F.; Wei, Y.; Vedadi, M.; Aebersold, R.; Wang, Y.; Houliston, S.; Arrowsmith, C. H. The MLL1 trimeric catalytic complex is a dynamic conformational ensemble stabilized by multiple weak interactions. *Nucleic Acids Res.* **2019**, *47* (17), 9433−9447.
(31) Avdic, V.; Zhang, P.; Lanouette, S.; Groulx, A.; Tremblay, V.; Brunzelle, J.; Couture, J. F. Structural and biochemical insights into MLL1 core complex assembly. *Structure* **2011**, *19* (1), 101−8.
(32) Xue, H.; Yao, T.; Cao, M.; Zhu, G.; Li, Y.; Yuan, G.; Chen, Y.; Lei, M.; Huang, J. Structural basis of nucleosome recognition and modification by MLL methyltransferases. *Nature* **2019**, *573* (7774), 445−449.
(33) Li, Y.; Han, J.; Zhang, Y.; Cao, F.; Liu, Z.; Li, S.; Wu, J.; Hu, C.; Wang, Y.; Shuai, J.; Chen, J.; Cao, L.; Li, D.; Shi, P.; Tian, C.; Zhang, J.; Dou, Y.; Li, G.; Chen, Y.; Lei, M. Structural basis for activity regulation of MLL family methyltransferases. *Nature* **2016**, *530* (7591), 447−52.
(34) Dou, Y.; Milne, T. A.; Ruthenburg, A. J.; Lee, S.; Lee, J. W.; Verdine, G. L.; Allis, C. D.; Roeder, R. G. Regulation of MLL1 H3K4 methyltransferase activity by its core components. *Nat. Struct. Mol. Biol.* **2006**, *13* (8), 713−9.
(35) Wan, X.; Hu, B.; Liu, J. X.; Feng, X.; Xiao, W. Zebrafish mll gene is essential for hematopoiesis. *J. Biol. Chem.* **2011**, *286* (38), 33345−57.
(36) Paffett-Lugassy, N. N.; Zon, L. I. Analysis of hematopoietic development in the zebrafish. *Methods Mol. Med.* **2004**, *105*, 171−98.
(37) Hanson, R. D.; Hess, J. L.; Yu, B. D.; Ernst, P.; van Lohuizen, M.; Berns, A.; van der Lugt, N. M.; Shashikant, C. S.; Ruddle, F. H.; Seto, M.; Korsmeyer, S. J. Mammalian Trithorax and polycomb-group homologues are antagonistic regulators of homeotic development. *Proc. Natl. Acad. Sci. U. S. A.* **1999**, *96* (25), 14372−7.
(38) Milne, T. A.; Briggs, S. D.; Brock, H. W.; Martin, M. E.; Gibbs, D.; Allis, C. D.; Hess, J. L. MLL targets SET domain methyltransferase activity to Hox gene promoters. *Mol. Cell* **2002**, *10* (5), 1107−17.
(39) Pearson, A. R.; Mehrabi, P. Serial synchrotron crystallography for time-resolved structural biology. *Curr. Opin. Struct. Biol.* **2020**, *65*, 168−174.
(40) Schapira, M.; Tyers, M.; Torrent, M.; Arrowsmith, C. H. WD40 repeat domain proteins: a novel target class? *Nat. Rev. Drug Discovery* **2017**, *16* (11), 773−786.

https://doi.org/10.1021/acscentsci.1c00434
ACS Cent. Sci. 2022, 8, 57−66